



Integrated Project - EUWB

Contract No 215669

Deliverable

D8b.3

System Simulation Environment

Contractual data:	M35
Actual data:	M37
Authors:	Stefan Gaier, Mohammed Alolofi, Alex Viessmann, Guido H. Bruck, Peter Jung, Andreas Waadt
Participants:	BOSCH, UDE
Work package:	WP8b
Security:	PU
Nature:	Report
Version:	1.0
Total number of pages:	28

Abstract

This report describes the simulation environment for impulse radio (IR)-Ultra-Wideband (UWB). The simulator contains the UWB channels in the EUWB automotive environment applications as they were modelled and described in deliverable D8b.4. After description of the developed simulator, performance results are presented, which were acquired with the simulator.

Keywords

Automotive, channel model, Impulse Radio (IR), Low Data Rate (LDR), software simulations, Ultra-Wideband (UWB).

Table of Contents

1 Executive Summary	5
2 Scenarios	6
2.1 Introduction	6
2.2 EUWB Channel Models for Automotive Environments	6
2.2.1 Overview	6
2.2.2 Tag Inside a Car in Open Space (CM8201)	7
2.2.3 Tag Outside a Car in Open Space (CM8202)	7
2.2.4 Tag Inside a Car in a Garage (CM8203)	7
2.2.5 Intrusion Detection (CM8204)	8
2.2.6 Cabin-Engine Com-Link (CM8205)	8
2.3 UWB Channels from IEEE According to 802.15 for Performance Evaluation of EUWB Channel Models	8
3 System Simulation Environment	9
3.1 Overview	9
3.2 Simulation Software	10
3.3 System Parameters	13
3.4 Spreading	14
3.5 Coherent Differential Binary Phase Shift Keying	15
3.6 Non-orthogonal Pulse Position Modulation	16
4 UWB Channels	17
5 Simulations	21
5.1 Settings	21
5.2 Simulation Results	21
5.3 Discussion	25
6 Conclusion	27
References	28
Acknowledgement	28

List of Figures

Figure 2-1: Example ID code of EUWB channel model.....	7
Figure 3-1: Flow chart diagram of the LDR UWB simulator	10
Figure 3-2: Software simulation environment.....	12
Figure 3-4: PN sequence	15
Figure 3-5: Auto-correlation function of the PN sequence	15
Figure 3-6: Differential encoded PN sequences of logical ‘0’ and ‘1’.....	16
Figure 4-1: Flow chart diagram of the UWB channel simulator [6]	19
Figure 5-1: Uncoded chip error ratio for coherent BPSK Rx.....	22
Figure 5-2: Uncoded chip error ratio for non-coherent Rx with differentially pre-encoded DBPSK... ..	22
Figure 5-3: Coded bit error ratio for non-coherent Rx with hard decision (HD) decoder, spreading factor $N_{PN}=12$, differentially pre-encoded DBPSK.....	23
Figure 5-4: Coded bit error ratio for non-coherent Rx with soft decision (SD) decoder, spreading factor $N_{PN}=12$, differentially pre-encoded DBPSK	23
Figure 5-5: Uncoded block error ratio for coherent BPSK Rx, block length $N_c=3072$	24
Figure 5-6: Uncoded block error ratio for non-coherent Rx, differentially pre-encoded DBPSK, block length $N_c=3072$	24
Figure 5-7: Coded block error ratio for non-coherent DBPSK Rx with hard decision (HD) decoder, spreading factor $N_{PN}=12$, block length $N_c=3072$	25
Figure 5-8: Coded block error ratio for non-coherent DBPSK Rx with soft decision (SD) decoder, spreading factor $N_{PN}=12$, block length $N_c=3072$	25

List of Tables

Table 3-1: Simulation system parameters	13
Table 4-1: Channel parameters for channel models of the EUWB automotive cluster WP8b [8].....	18
Table 4-2: Channel parameters for standard IEEE 802.15 channel models CM1-4 [4].....	18

Abbreviations

ACF	Autocorrelation function
ADC	Analogue to digital converter
AWGN	Additive white Gaussian noise
BER	Bit error ratio
BLER	Block error ratio
BPSK	Binary phase shift keying
CIR	Channel impulse response
DBPSK	Differential binary phase shift keying
EUWB	CoExisting Short Range Radio by Advanced Ultra-WideBand Radio Technology
HD	Hard decision
ID	Identity
IR	Impulse radio
ISI	Inter-symbol interference
LDR	Low data rate
MF	Matched filter
NRZ	Non return to zero
N-PPM	Non-orthogonal pulse position modulation
PDP	Power delay profile
PN	Pseudo noise
PPM	Pulse position modulation
PRI	Pulse repetition interval
PRP	Pulse repetition period
RF	Radio frequency
SD	Soft decision
SRN	Signal to noise ratio
UWB	Ultra-wideband

1 Executive Summary

This report presents a software simulation environment. The software simulator includes UWB channels according to the channel models, which were developed after channel measurements in the EUWB automotive environment. The measurement conditions during the channel characterization and the channel models, implemented in the software simulator, are based on application scenarios, which were defined in D8b.1 [3]. The channel models are therefore tailored to the automotive cluster. Chapter 2 gives an introductory overview of the different scenarios.

The UWB transceivers, which are used in the automotive cluster, are using low data rate (LDR) impulse radio (IR)-ultra-wideband (UWB) platforms. Their characteristics have been implemented in the software simulator and are described in chapter 3.

The developed software simulator has been used to carry out link level simulations using the different modulation schemes of the LDR platforms in different channel models. The channel models represent the different application scenarios of the automotive cluster WP8b. The implementation details of the channel models in the simulator are described in chapter 4.

To allow the comparison with commonly known UWB channel models, which are defined in IEEE 802.15 [4], the performance of the LDR platform has also been simulated using standardized UWB channels. Both simulation results from the standardized IEEE 802.15 channels and from the WP8b channels are presented and discussed in chapter 5.

Chapter 6 concludes this report.

2 Scenarios

2.1 Introduction

For the characterization of the UWB mobile channel, channel measurements in the automotive environment were carried out by BOSCH within the EUWB work package cluster WP8b. The measurements' outcome was used to parameterize UWB channel models, which are based on the Saleh-Valenzuela model [5]. The fundamental model and channel simulation framework is described in D8b.4 [6]. The measurement equipment and the channel measurement setups are described in D3.1.2b [7]. The measurement results and the corresponding parameterization of the channel models in the automotive environment is described in D8b.5 [8]. Section 2.2 introduces the scenarios, defined in D8b.1 [3], which were the basis for the measurements and which are represented by the different channel models.

The parameters of the EUWB channel models are comparable with the UWB channel models from IEEE 802.15, cf. section 2.3 [4]. The IEEE UWB channel models are based on measurements by the IEEE channel modelling sub-committee in IEEE P802.15-02/240-SG3a [9],[10].

The simulation software, described in this report, allows simulations in both the EUWB channel models and the IEEE UWB channel models. Furthermore, the simulator includes the system model of the EUWB low data rate (LDR) platform, which is specified in D7.1.1b [11], cf. chapter 4.

2.2 EUWB Channel Models for Automotive Environments

2.2.1 Overview

The channel measurements from D8b.5 were evaluated to parameterize five different channel models. These channel models are in particular:

- CM8201 (tag inside a car in open space),
- CM8202 (tag outside a car in open space),
- CM8203 (tag inside a car in a garage),
- CM8204 (intrusion detection), and
- CM8205 (cabin-engine com-link).

The identity (ID) code of the channel models are composed of the following parts:

1. two letters ("CM"), standing for "channel model",
2. four digits (e.g. "8205"), representing the number of the channel model.

This ID composition is compatible with the channel model IDs in IEEE 802.15, cf. section 2.3 [4].

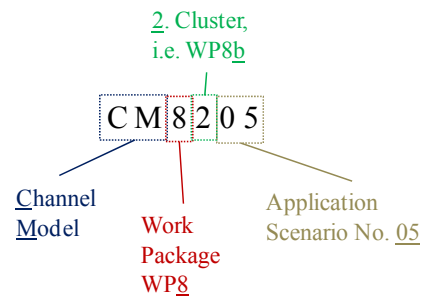


Figure 2-1: Example ID code of EUWB channel model

Figure 2-1 shows the composition of the EUWB channel model IDs in more detail. The four digits number (2) is further subdivided into

- a) one digit (“8”) for the work package in EUWB,
- b) one digit (“2”) for the cluster, e.g. cluster b), automotive,
- c) two digits (“e.g. “05”) for the application scenario.

The five channel models CM8201-CM8205 are based on 78 measurement setups, which were grouped into 5 major groups of application scenarios. The measurement results of one application scenario share certain statistical properties. These statistics completely describe the properties of impulse responses for stationary channels. During the software simulations, the channel impulse responses (CIR) are randomly generated from the statistical parameters of the five channel models. The five application scenarios, represented by the five channel models, are described in section 2.2.2-2.2.6. The exact mapping of the 78 measurement setups to the five channel models is detailed in section 4.5 and Table 3-3 of D8b.5 [8], and in chapter 4 of D3.1.2b [7].

2.2.2 Tag Inside a Car in Open Space (CM8201)

The EUWB channel model CM8201 is tailored to the mobile UWB channel between a mobile tag, which is located inside a car in open space, and an anchor node, which is mounted inside the car. Possible locations inside the passenger cabin are at the ceiling, at one of the a-pillars at the ceiling inside the passenger compartment, the dashboard near the front a-pillars, at a side pillar, the rear view mirror, or at the canopy. The mobile tag is located for measurements at the front-seat, or at the right rear-seat, about 80cm below the antennas at the ceiling. The car is not surrounded by any obstacles, cf. section 4.5.2 in D8b.5 [8].

2.2.3 Tag Outside a Car in Open Space (CM8202)

The channel model CM8202 is tailored to channels between a mobile tag, which is located outside a car in open space, and an anchor node, which is mounted inside the car. Also in this scenario, the car is not surrounded by any obstacles. The locations of the anchors are the same like in CM8201. The tag location may be in front of the car, right beside the car, or behind the car, cf. section 4.5.3 in D8b.5 [8].

2.2.4 Tag Inside a Car in a Garage (CM8203)

The channel model CM8203 is similar to CM8201; it describes channels between a mobile tag inside a car and a fixed installed anchor node. In contrast to CM8201, the CM8203 is tailored to scenarios, where the car is in a garage and surrounded by other cars, cf. section 4.5.4 in D8b.5 [8].

2.2.5 Intrusion Detection (CM8204)

The channel model CM8204 is tailored to scenarios of passive location tracking (LT), therefore UWB transceivers are mounted at the fixed installed anchor node positions described in CM8201, and with a human obstacle, which is approaching from the rear or from the car's side. The mobile channels, described by CM8204, are the channels between the anchor nodes. These mobile channels are affected by the approaching intruder, cf. section 4.5.5 in D8b.5 [8], and section 4.1.7 of D3.1.2b [7].

2.2.6 Cabin-Engine Com-Link (CM8205)

The EUWB channel model CM8205 is tailored to mobile channels between stationary UWB nodes in the engine compartment and the cabin of the car, cf. section 4.5.6 in D8b.5 [8], and section 4.1.8 of D3.1.2b [7].

2.3 UWB Channels from IEEE According to 802.15 for Performance Evaluation of EUWB Channel Models

UWB channels had been defined in the past. After measurements by the IEEE channel modelling sub-committee in IEEE P802.15-02/240-SG3a, IEEE 802.15 defined four UWB channel models [4]. They are:

- CM1: a measurement based line of sight (LOS) channel with distances of $d = 0-4$ m,
- CM2: a measurement based non-line of sight (NLOS) channel with distances of $d = 0-4$ m,
- CM3: a measurement based NLOS channel with distances of $d = 4-10$ m,
- CM4: a theoretically constructed extreme NLOS channel with a root mean square (RMS) delay spread of $\tau_{\text{rms}} = 25$ ns.

CM1 and CM2 are based on measurements in [9]. CM3 is based on measurements from [9] and [10]. CM4 is a theoretical channel.

3 System Simulation Environment

3.1 Overview

This chapter describes the system simulation environment. An overview of the simulator's functions is given in the flow chart diagram in Figure 3-1. Key components are the transceiver and the UWB channel model. The UWB channels are generated by a channel simulator module, which was introduced in D8b.4 [6], and is briefly described in chapter 4. This chapter is focusing on the transceiver, i.e. the system architecture for the Impulse Radio - Ultra Wideband (IR-UWB) Low Data Rate - Location and Tracking (LDR-LT) platform, which is described comprehensively and with respect to the implementation in the software simulator. A detailed description of the requirements and specification of the LDR platform along with feasibility analysis is given in D7.1.1b [11].

The IR-UWB uses short energy pulses for transmitting the information symbols. The pulses have a broad bandwidth and a duration, which is short compared to their temporal distance, i.e. the pulse repetition period. The nature of the signals offer a high robustness to multipath propagation and frequency selectivity. Several modulation schemes have been defined such as pulse position modulation (PPM) and Phase Shift Keying (PSK). The generated pulses can be Gaussian or one of its n 'th derivatives. To spread the bit energy over a broad bandwidth and to allow flexible data rates at a reliable link quality, the bits are spread, or encoded, with Pseudo Noise (PN) sequences of variable length.

The performance of the IR-UWB system depends on the receiver structure. The receiver structure can be categorized to coherent and non-coherent receivers. Comparable to a rake receiver, the coherent receiver detect the polarity of pulses received. Compared to a non-coherent receiver, the coherent receiver can provide lower bit error ratios (BER) at expense of more complexity and higher power consumption.

The coherent approach uses a coherent differential binary phase shift keying (DBPSK) referred to as differentially coherent DBPSK, cf. section 3.5. The non-coherent approach uses non-coherent non-orthogonal pulse position modulation (N-PPM), cf. section 3.6. Frequency spreading is used to spread from a variable bit rate to a fixed chip rate of 1 GHz, cf. section 3.4. The possible data rates and corresponding spreading factors are described in section 3.3 along with the other system simulation parameters.

Both receiver structures implement a frequency de-spreading by correlation with the utilized PN sequence. The bit detection at the correlator's output can be done with two strategies: either soft detection (SD) or hard detection (HD). In case of a hard decision demodulator, the chip signal is first quantized to 1 bit before the correlation is carried out. Else, if using soft decision, the signal is first de-spread before the correlator's output is quantized to 1 bit. The SD receiver shows a better performance than the HD receiver, cf. chapter 5.

3.2 Simulation Software

Figure 3-1 depicts the flow chart diagram of the simulation software.

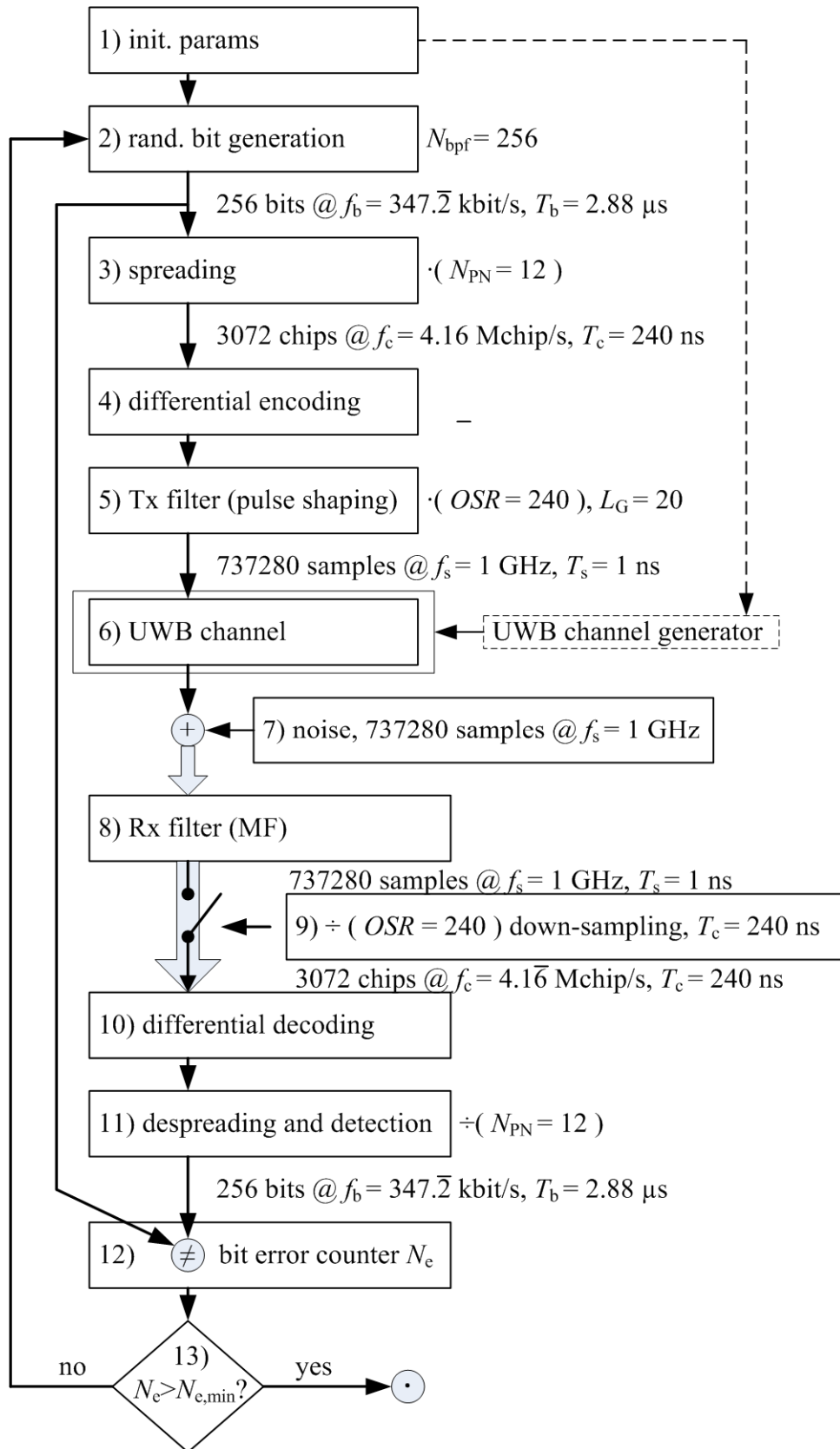


Figure 3-1: Flow chart diagram of the LDR UWB simulator

The simulation can be described by 13 functions. They are:

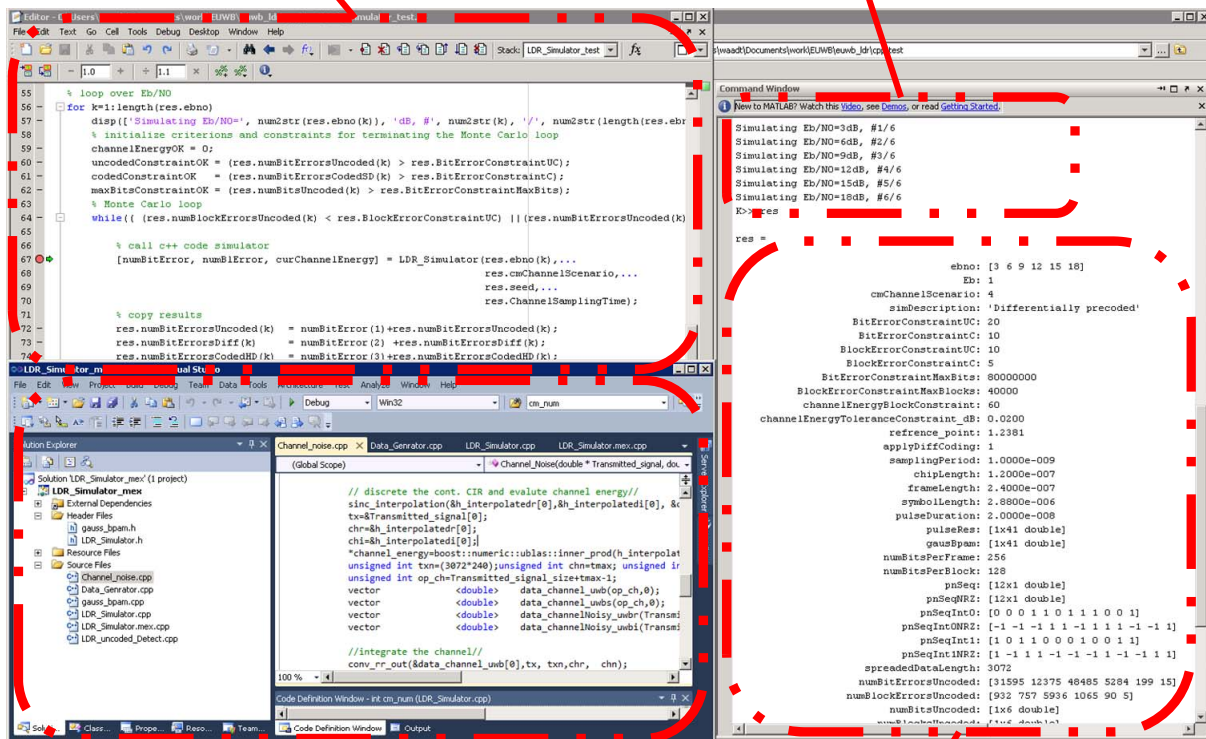
- 1) Parameter initialization: The system simulation parameters are specified on the top of the main MATLAB script of the simulation software. After initialization, the simulation is running in a C++ implementation of a MATLAB MEX routine.
- 2) Random bit generation: Frames of $N_{\text{bpf}} = 256$ random bits per frame (bpf) are generated by a pseudorandom number generator. The bit rate is between $f_{\text{b,min}} = 134$ kbit/s and $f_{\text{b,max}} = 4166$ kbit/s. Typically it is about $f_{\text{b}} = 347$ kbit/s.
- 3) Spreading: The bits are spread with a pseudo noise (PN) sequence. Depending on the wanted data rate, the PN sequence length may be between $N_{\text{PN,min}} = 1$ and $N_{\text{PN,max}} = 16$. The typical value is $N_{\text{PN}} = 12$. The resulting chip stream has a chip rate of $f_{\text{c}} = 4.166$ Mchip/s. The chip period is therefore $T_{\text{c}} = 1/f_{\text{c}} = 240$ ns.
- 4) Differential encoding: The chip stream is differentially encoded. Depending on the simulation settings, this function can optionally be disabled.
- 5) Tx filtering: In the transmission (Tx) filter function, Gaussian shaped pulses of a duration of $T_{\text{G}} = 20$ ns are generated for every chip. The filter's impulse response is described in (3.1) and shown in Figure 3-3. The system sampling rate is $f_{\text{s}} = 1$ GHz. Hence, every chip of duration $T_{\text{c}} = 240$ ns is represented by 240 samples with the sample period $T_{\text{s}} = 1/f_{\text{s}} = 1$ ns. Since the pulse duration T_{G} of the transmission filter is smaller than the chip period $T_{\text{c}} > T_{\text{G}}$, the chips do not overlap. Thus, there will be no inter-symbol interference (ISI) in a perfect additive white Gaussian noise (AWGN) channel.
- 6) UWB channel: The digital signal is convolved with the channel impulse response of the UWB channel. The channel impulse response is generated by a UWB channel generator module, which is described in chapter 4. It includes time variance and fading. The channel is simulated in the equivalent baseband, i.e. the signal is not mixed up to the radio frequency (RF).
- 7) Noise: White Gaussian noise is generated and added to the received signal at the channel's output. The noise variance depends on the signal to noise ratio (SNR) to be simulated.
- 8) Rx filter: Since the simulation is carried out in the equivalent baseband, the receiver does not include a band selection filter in the RF. A low pass filter is used instead. The utilized receiver low pass filter is a matched filter (MF) to the Tx filter, cf. (3.1) and Figure 3-3.
- 9) Down-sampling: The Rx filter's output signal of $f_{\text{s}} = 1$ GHz sample rate is down-sampled by a factor of 240. I.e. one sample is taken for every chip. The resulting chip rate is $f_{\text{c}} = 4.166$ Mchip/s.
- 10) Differential decoding: The chip signal is differentially decoded. Depending on the simulation settings, this function can optionally be disabled.
- 11) De-spreading & detection: The chip signal is correlated with the spreading sequence and down-sampled to the bit rate. Depending on the simulation settings, the simulator will first quantize the chip signal, before the correlation is carried out. This method is referred to as hard decision (HD) de-spreading. Else it is soft decision (SD) de-spreading. The output of the de-spreading correlator and down-sampling unit is fed into a thresholds decision unit, which detects the bits.

- 12) Evaluation: The bits, detected in the receiver's de-spreading & detection function are compared with the originally transmitted bits from the transmitter's random bit generation function. The number N_e of bit errors are counted as well as the total number N_{tot} of simulated, transmitted bits. The *coded* bit error ratio (BER) is the ratio of bit errors N_e and transmitted bits N_{tot} . The number of chip errors are counted as well to evaluate the *uncoded* BER or chip error ratio. Finally, the block error ratio (BLER) is the ratio of number of simulated frames with at least one bit error and the total number of simulated frames.
- 13) Termination: The simulation, described in steps 1)-12) is repeated in outer loops over the SNR and inner Monte Carlo loops. There are several abort criterions and constraints for the termination of the Monte Carlo loop:
- The Monte Carlo simulation continues if the difference between the averaged, normalized channel power P_c and the nominal channel power exceeds a threshold Γ_c .
 - The simulation terminates if the total number N_{tot} of simulated bits exceeds a predefined threshold Γ_{tot} , and constraint a is satisfied.
 - It terminates if the number N_e of bit errors exceeds a predefined threshold Γ_e , and constraint a is satisfied.

After termination, the simulation results are returned from the C++ MEX routine to MATLAB and can be graphically displayed. Simulation results are shown in chapter 5.

Matlab program for parameter settings, result evaluation and visualization

Matlab console with simulation progress information



C++ project of MEX-file (dynamic link library)

typical simulation result set

Figure 3-2: Software simulation environment

Figure 3-2 shows the software simulation environment. It consists of a MATLAB script and a C++ project for the development of the MATLAB MEX-file.

3.3 System Parameters

The main system simulation parameters are summarized in Table 3-1. The chip period T_c is also referred to as pulse repetition period (PRP), since the chips are represented by pulses as depicted in Figure 3-3. Half of a transmitted pulse is positive, whereas the other half is negative. A half pulse is also referred to as sub-chip. The sub-chip length is $T_{sc} = T_c/2 = 120$ ns.

Table 3-1: Simulation system parameters

	min. rate	typical rate	max. rate
gross bit rate f_b	134 kbit/s	347 kbit/s	4166 kbit/s
bit period T_b	7.44 μ s	2.88 μs	0.24 μ s
PN sequence length N_{PN}	16	12	1
chip period T_c		240 ns	
pulse duration T_G		20 ns	
sampling period T_s		1 ns	

During the simulation, the number of bits per frame was always $N_{bpf} = 256$. With N_{bpf} and with the PN sequence length N_{PN} , the number of chips per frame becomes $N_c = N_{bpf} \cdot N_{PN}$. With the constant chip period T_c the frame length becomes $T_{frame} = N_c \cdot T_c$. In the simulation, every chip is represented by 240 samples with sample period $T_s = 1$ ns.

The Gaussian pulses, which are transmitted with the chip period $T_c = 240$ ns, can be described by

$$g(t) = \frac{-\frac{t}{\sigma^2} \cdot \frac{1}{\sqrt{2\pi\sigma}} \exp\left(\frac{-t^2}{2\sigma^2}\right)}{\sqrt{\int_{-\infty}^{\infty} \left[-\frac{t}{\sigma^2} \cdot \frac{1}{\sqrt{2\pi\sigma}} \exp\left(\frac{-t^2}{2\sigma^2}\right)\right]^2}}, \quad \sigma = \frac{T_G}{2\pi}. \quad (3.1)$$

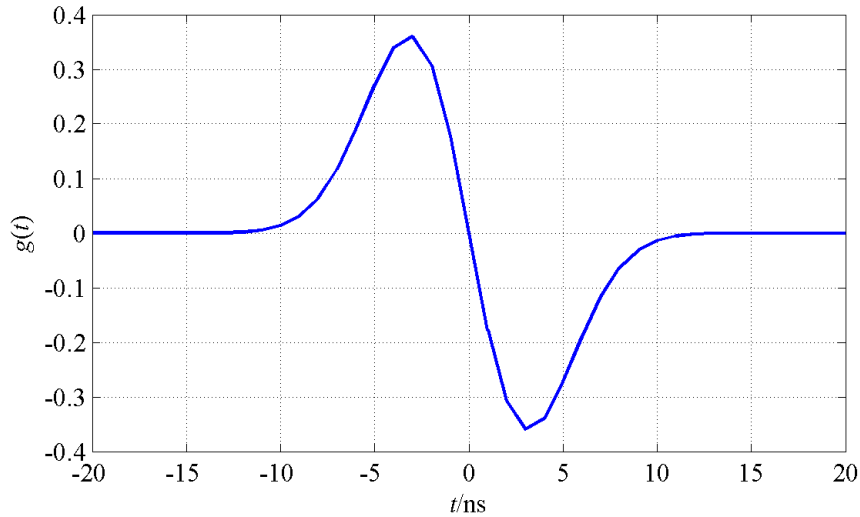


Figure 3-3: Derivative of Gaussian pulse for LDR UWB

The Gaussian pulse in (3.1) is normalized to a chip energy of 1. The parameter T_G in (3.1) is the duration of the Gaussian pulse. In fact, $g(t)$ in (3.1) has an infinite duration. However, more than 99.9 % of the pulse energy is covered within a duration of T_G . In the simulator, the Gaussian pulse is truncated to a length of 40 ns. The Gaussian pulse can also be used as a matched filter (MF) in the receiver. In case of correctly synchronized down-sampling of the filter's output, this will concentrate the received signal's energy in the points in time of the sampling and, thus, maximize the signal to noise ratio (SNR).

3.4 Spreading

The data bits are spread with PN sequences of sequence length $N_{PN} \in [1;16]$. Every chip of a PN sequence is represented by a pulse as depicted in Figure 3-3. The typical PN sequence length is $N_{PN} = 12$. Equation (3.2) shows the PN sequence of length $N_{PN} = 12$:

$$\mathbf{s}_{PN} = (1,1,1,0,1,0,0,1,1,0,1,0). \quad (3.2)$$

Binary phase shift keying (BPSK) uses symbols with different phases but with same amplitudes. The resulting BPSK signal can therefore be seen as a non-return-to-zero (NRZ) signal. Figure 3-4 shows a NRZ representation of the typical PN sequence of length $N_{PN} = 12$. A '+1' in Figure 3-4 represents a logical '1' in (3.2), whereas a '-1' in Figure 3-4 represents a logical '0' in (3.2). The sequence \mathbf{s}_{PN} will be transmitted instead of a logical '1'. If a logical '0' shall be transmitted, the inverted sequence $-\mathbf{s}_{PN}$ will be transmitted.

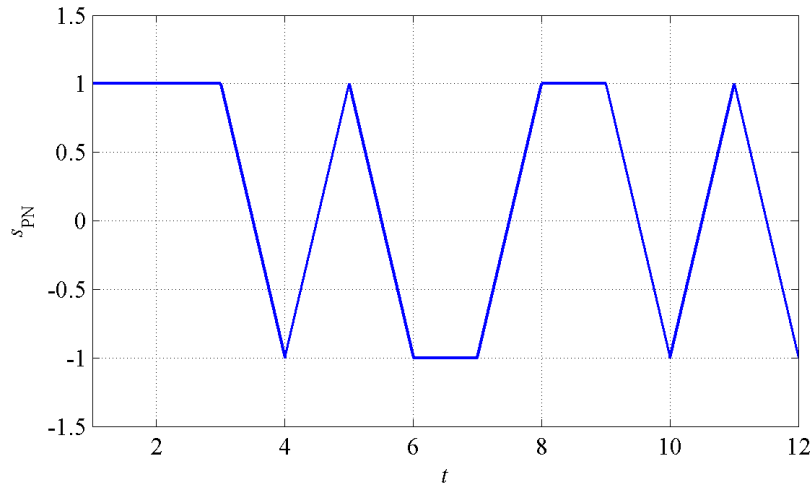


Figure 3-4: PN sequence

In the receiver, the received and MF filtered signal is correlated with the PN sequence. The correlator's output signal is the autocorrelation function (ACF) of the PN sequence. Figure 3-5 shows the autocorrelation function of the NRZ version of the PN sequence used by the sensor hardware from CEA-LETI. The PN sequence's energy is concentrated in the middle of the ACF. In case of correctly synchronized sampling, the resulting bit energy to noise ratio E_b/N_0 will be by a factor of N_{PN} larger than the chip energy to noise ratio E_c/N_0 :

$$10 \cdot \log_{10} \left(\frac{E_b}{N_0} \right) = 10 \cdot \log_{10} \left(\frac{E_c}{N_0} \right) + \underbrace{10 \cdot \log_{10} (N_{PN})}_{\approx 10.8 \text{ dB} |_{N_{PN}=12}}. \quad (3.3)$$

For $N_{PN} = 12$, for instance, the chip energy to noise ratio E_c/N_0 will be by about 10.8 dB smaller than the bit energy to noise ratio E_b/N_0 .

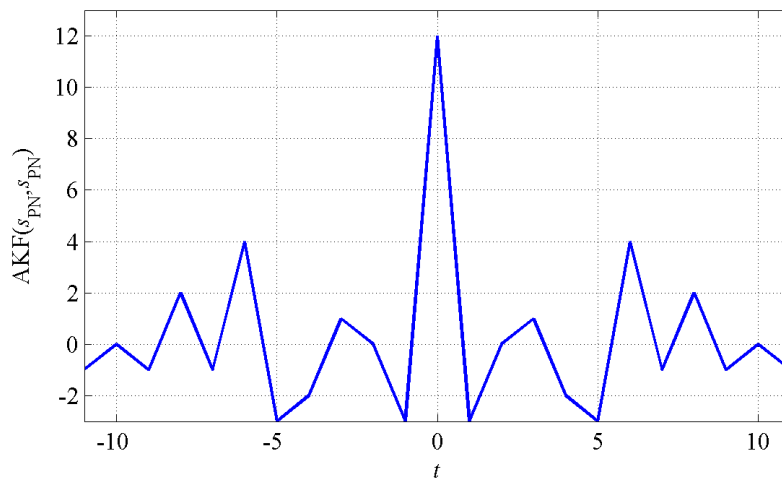


Figure 3-5: Auto-correlation function of the PN sequence

3.5 Coherent Differential Binary Phase Shift Keying

The differentially coherent DBPSK transceivers use differential binary phase shift keying (DBPSK) and frequency spreading. DBPSK uses a differential pre-encoding. Starting from a logical '0', i.e. a signal level of '-1', the differentially encoded signal does not change its value, if a logical '0' is

transmitted. If however a logical ‘1’ is transmitted, the signal value changes either from ‘-1’ to ‘+1’ or vice versa. Figure 3-6 shows the differentially encoded PN sequences from (3.2) and Figure 3-4 of logical ‘0’ (blue graph) and ‘1’ (red dashed graph).

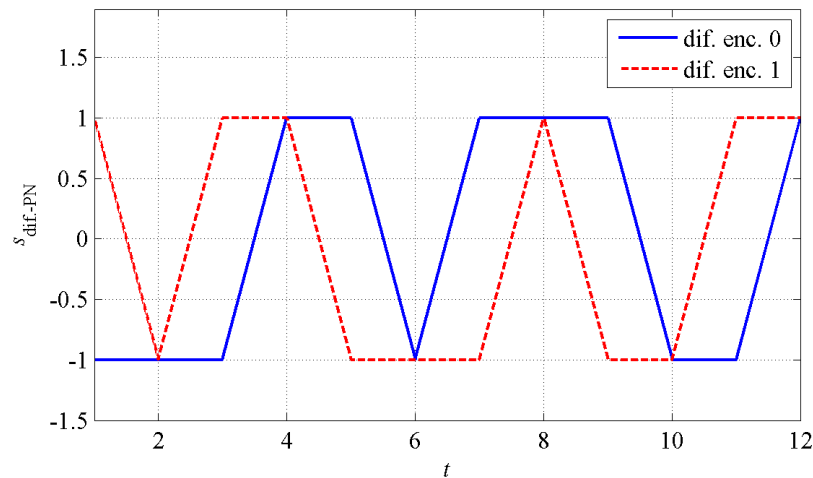


Figure 3-6: Differential encoded PN sequences of logical ‘0’ and ‘1’

Differentially coherent DBPSK receivers (RX) subsample the incoming radio frequency (RF) signal. Due to the subsampling, no additional down-conversion unit is required. The demodulation of the data symbols is done differentially. For this purpose a differential antenna is used, which provides two versions of the received signal. After subsampling and analogue to digital conversion (ADC), an energy detection module combines the two received digital signals in a XNOR gate. The output of the XNOR gate is 1, if the signals are the same, and 0 otherwise. This XNOR output is then multiplied with one of the received digital signals, yielding a 3-level signal, also referred to as 1.5-bit signal. The 3 signal levels are $\{-1, 0, +1\}$. This sampling principle had first been introduced in [12]. This demodulation structure benefits from its simplicity and low power consumption at low data rates. However, a disadvantage, compared to classical analogue non-coherent receivers, is certain performance degradation.

3.6 Non-orthogonal Pulse Position Modulation

When assuming good synchronization and equalization, differential pre-encoding doubles the number of bit errors compared to modulation schemes, which do not use differential pre-encoding. Reason for this are the inherited errors, which result from previous symbol detection errors. This property of the DBPSK can also be observed in the simulation results on chapter 5. However, the inherited errors do not effect the block error ratio (BLER), since one bit error is sufficient to yield a block error, independently in the number of inherited errors.

An alternative modulation scheme, which does not use any differential pre-encoding is the non-coherent non-orthogonal pulse position modulation N-PPM. In case of non-coherent N-PPM, the demodulation can be performed using the “energy” output alone.

4 UWB Channels

One central function of the software simulator, introduced in chapter 3, is the function 6), UWB channel. The channel is in principal linearly modelled and described by a channel impulse response

$$h(\tau) = \sum_{i=0}^{\infty} \beta_i \cdot e^{j\Theta_i} \delta(\tau - \tau_i), \quad (4.1)$$

with the Dirac delta function $\delta(\tau)$, with path delays τ_i , with path gains β_i , and with different zero phase angles, caused by different phase shifts Θ_i of the channel's paths. The parameters $\tau_i(t)$, $\beta_i(t)$, and $\Theta_i(t)$ are generally time variant, yielding a time variant channel impulse response $h(\tau, t)$. In the software simulator, the channel impulse response is periodically generated by the UWB channel generator, including time variations of the parameters $\tau_i(t)$, $\beta_i(t)$ and $\Theta_i(t)$, as well as log normal fading on the channel energy

$$E_h(t_1) = \int_{\tau=0}^{\infty} \|h(\tau, t_1)\|^2 d\tau. \quad (4.2)$$

The channel is simulated in the equivalent baseband, i.e. signals are not mixed up to the RF. The received signal $v(t)$ at the channel's output becomes the convolution of the transmitted signal $u(t)$ and the channel impulse response.

The channel impulse responses are randomly generated. Thus, the parameters τ_i , β_i , and Θ_i are random variables. However, since the channel is assumed to be quasi-stationary, the stochastic parameters of the channel's power delay profile (PDP) are fixed defined by the channel model or the simulation scenario, cf. chapter 2.

The channel models are based on a Saleh Valenzuela (S-V) channel model. The channel impulse response $h(t)$ is composed to clusters of rays. The arrival rates of both clusters and rays within the clusters are Poisson distributed on the τ -axis. Thus, the inter-arrival times, i.e. the time differences $\Delta\tau$ between temporally adjacent clusters or between temporally adjacent rays, are exponentially distributed. Characteristic parameter of the Poisson distribution of the clusters is the mean cluster arrival rate Λ . Characteristic parameter of the cluster's power distribution is the cluster decay time Γ . Correspondingly, the characteristic parameters of the distribution of the rays and their amplitudes are the ray arrival rate λ and the ray decay time γ . The phase angles of the rays are uniformly distributed, $\Theta \in [0, 2\pi)$.

The characteristic parameters, Λ (cluster arrival rate), λ (ray arrival rate), Γ (cluster decay time), and γ (ray decay time) are found after measurements of the PDP. For an infinite number of clusters and rays, the PDP can generally be written as

$$\overline{\beta^2(\tau)} = \overline{\beta_{00}^2} \cdot \sum_{l=0}^{\infty} e^{-T_l/\Gamma} e^{-(\tau-T_l)/\gamma} U(\tau - T_l), \quad (4.3)$$

with the ray gain β_{00} of the 1st ray in the 1st cluster, the delay T_l of the $(l-1)$ th cluster, the cluster decay time Γ , the ray decay time γ , and with the Heaviside step function $U(\tau)$.

Measurements to determine the characteristic parameters had been carried out and described in D8b.5 for the five different automotive EUWB environments and scenarios [8]. They are summarized in Table 4-1. Similar sets of those parameters had also been determined for four different indoor scenarios by IEEE. They are summarized in Table 4-2. The software simulator, described in chapter 3 includes the nine channel models from EUWB and IEEE.

Table 4-1: Channel parameters for channel models of the EUWB automotive cluster WP8b [8]

Channel model Model parameters	CM8201 (tag inside a car in open space)	CM8202 (tag outside a car in open space)	CM8203 (tag inside a car in a garage)	CM8204 (intrusion detection)	CM8205 (cabin-engine com-link)
Cluster arrival rate	0.0212 ns ⁻¹	0.0226 ns ⁻¹	0.014 ns ⁻¹	0.0144 ns ⁻¹	0.0143 ns ⁻¹
Ray arrival rate	3.5985 ns ⁻¹	3.1625 ns ⁻¹	2.2487 ns ⁻¹	2.5901 ns ⁻¹	4.3032 ns ⁻¹
Cluster decay factor	11.2 ns	22.8 ns	14.9 ns	8.2 ns	8.1 ns
Ray decay factor	5.8 ns	8.3 ns	14.9 ns	5.6 ns	8.1 ns
Std. dev. of cluster fading	3.4 dB	3.4 dB	3.4 dB	3.4 dB	3.4 dB
Std. dev. of ray fading	3.4 dB	3.4 dB	3.4 dB	3.4 dB	3.4 dB
Std. dev. of total multipath fading	3 dB	3 dB	3 dB	3 dB	3 dB

Table 4-2: Channel parameters for standard IEEE 802.15 channel models CM1-4 [4]

Channel model	CM1	CM2	CM3	CM4
Cluster arrival rate	0.0233 ns ⁻¹	0.4 ns ⁻¹	0.0667 ns ⁻¹	0.0667 ns ⁻¹
Ray arrival rate	2.5 ns ⁻¹	0.5 ns ⁻¹	2.1 ns ⁻¹	2.1 ns ⁻¹
Cluster decay factor	7.1 ns	5.5 ns	14 ns	24 ns
Ray decay factor	4.3 ns	6.7 ns	7.9 ns	12 ns
Std. dev. of cluster lognormal fading	3.4 dB	3.4 dB	3.4 dB	3.4 dB
Std. dev. of ray lognormal fading	3.4 dB	3.4 dB	3.4 dB	3.4 dB
Std. dev. of lognormal fading for total multipath realizations	3 dB	3 dB	3 dB	3 dB

After loading the stochastic parameters from configuration header files, the described S-V model is used to generate the random variables

- T_l , the delay of the $(l+1)$ -th cluster,
- $\tau_{k,l}$, the delay of the $(k+1)$ -th ray within the $(l+1)$ -th cluster,
- $\beta_{k,l}$, the gain of the $(k+1)$ -th ray within the $(l+1)$ -th cluster, and
- $\Theta_{k,l}$, the phase shift of the $(k+1)$ -th ray within the $(l+1)$ -th cluster.

With these variables, the channel impulse response (CIR) is composed to

$$h(t) = \sum_{l=0}^{\infty} \sum_{k=0}^{\infty} \beta_{k,l} \cdot e^{j\Theta_{k,l}} \delta(t - T_l - \tau_{k,l}). \quad (4.4)$$

Figure 4-1 shows the flow chart diagram of the UWB channel simulator [6].

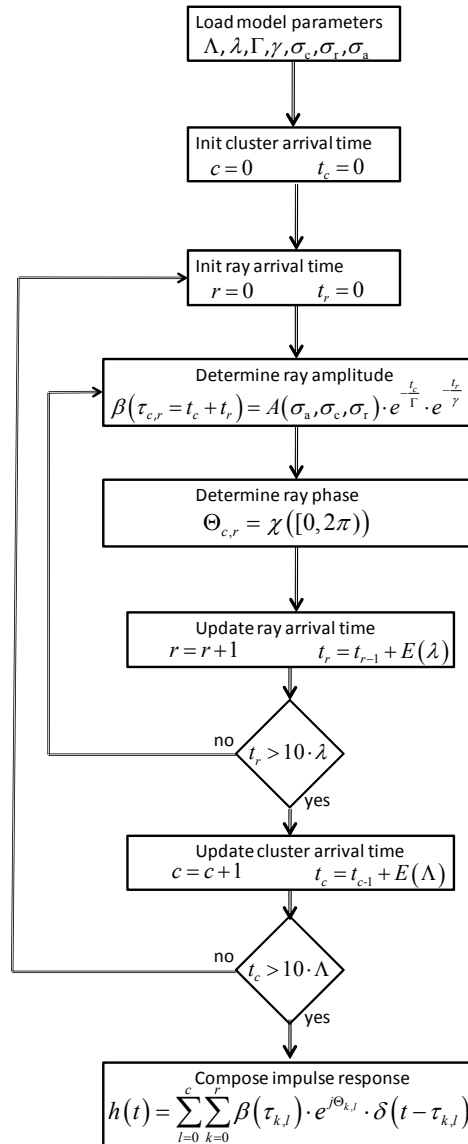


Figure 4-1: Flow chart diagram of the UWB channel simulator [6]

After sorting the rays, the CIR in (4.4) can also be written as described in (4.1). This generated CIR is irregularly sampled, since the delays $\tau_{k,l}$ and T_l are continuously distributed. However, since the software simulator is a digital simulator with a regular sampling period is $T_s = 1$ ns (cf. Table 3-1), a

regular sampled CIR is required. For this purpose, the regular samples are interpolated by a poly-phase filter of a bandwidth, which is equal to the system bandwidth of 1 GHz.

5 Simulations

5.1 Settings

The performance of the system has been elaborated in the EUWB automotive channel models CM8201 to CM8205 and in the standard IEEE 802.15.3a channel models CM1 to CM4. For each elaboration the bit error ratio (BER) and block error ratio (BLER) performances is obtained for the DBPSK modulation scheme as well as for BPSK without differential coding.

The random bits, generated on the receiver side, are segmented to 128-bit blocks, spread with the PN code from (3.2) and finally modulated with the DBPSK or BPSK modulation schemes. The differential encoder correlates the current bit and the previous output of the encoder using XOR logic operation. At the output of the modulator, the pulses are represented as two levels, -1 and +1, and up-sampled before pulse-shaped into a suitable waveform that complies with the FCC power limitation and the UWB emission mask. The pulse shaper processes pulses and sample to form the required third-derivative Gaussian waveform. The chip lengths, frame lengths and symbol lengths are 120 ns, 240 ns and 2.88 μ s, respectively. With the spreading factor of 12, the gross bit rate is 347 kbit/s.

The transmitted signal is convoluted with the multipath channel, generated from the channel generator. On the receiver side white Gaussian noise is added to the received signal. Receive filters are used. Assuming perfect channel knowledge and synchronization received signal is matched filtered with the current CIR. The resulting signal is convolved with the Gaussian filter to detect the energy of the signal pulses. Finally, the signal is down-sampled to a set of pulses, detected by a comparator. If soft detection (SD) de-spreading is used, the bit energy of a PN sequence is collected by a correlator before the bit value is decided. If hard detection (HD) de-spreading is used; the receiver performs N_{PN} independent decision on the N_{PN} chips, before the chips are summed up and the bit value is decided.

5.2 Simulation Results

Figure 5-1 to Figure 5-8 show performance simulation results of DBPSK and BPSK, coded and uncoded, with hard decision (HD) and soft decision (SD) despreading, with $N_{PN} = 12$ chips per bit. The block length was $N_b = 256$ bits per frame, if the performance was simulated with spreading (coded), or $N_C = 3072$ chips per block if the performance was simulated without spreading (uncoded). The ratio of the number N_b of bits and the number N_C of chips per frame is the spreading factor $N_C/N_b = N_{PN}$, i.e. the number of chips per bit.

Figure 5-1 and Figure 5-2 show the chip error ratio for coherent BPSK receivers (Rx) and non-coherent receivers with differentially pre-encoded DBPSK. The chip error ratio is equivalent to the uncoded bit error ratio (BER).

Figure 5-3 and Figure 5-4 show the coded bit error ratios (BER) of non-coherent receivers with differentially pre-encoded DBPSK. “Coded” means in this context that every bit is spread with $N_C = 12$ chips and despread in the receiver. Figure 5-3 shows the performance of a hard decision (HD) despreader (decoder), whereas Figure 5-4 shows the performance for a soft decision (SD) despreader (decoder). The BER is plotted over the bit energy to noise ratio $10 \cdot \log_{10}(E_b / N_0)$. The bit energy is equal to the energy of $N_C = 12$ chips \square 10.8 dB.

Figure 5-5 to Figure 5-8 show block error ratios. The uncoded block error ratios are shown in Figure 5-5 for the coherent BPSK receiver and in Figure 5-6 for the non-coherent receiver with differentially

pre-encoded DBPSK. The coded BLER performance is shown in Figure 5-7 and Figure 5-8, both for the non-coherent receiver with differentially pre-encoded DBPSK. The results in Figure 5-7 show the performance if a hard decision (HD) despreader (decoder) is used; in case of Figure 5-8 a soft decision (SD) despreader (decoder) is used.

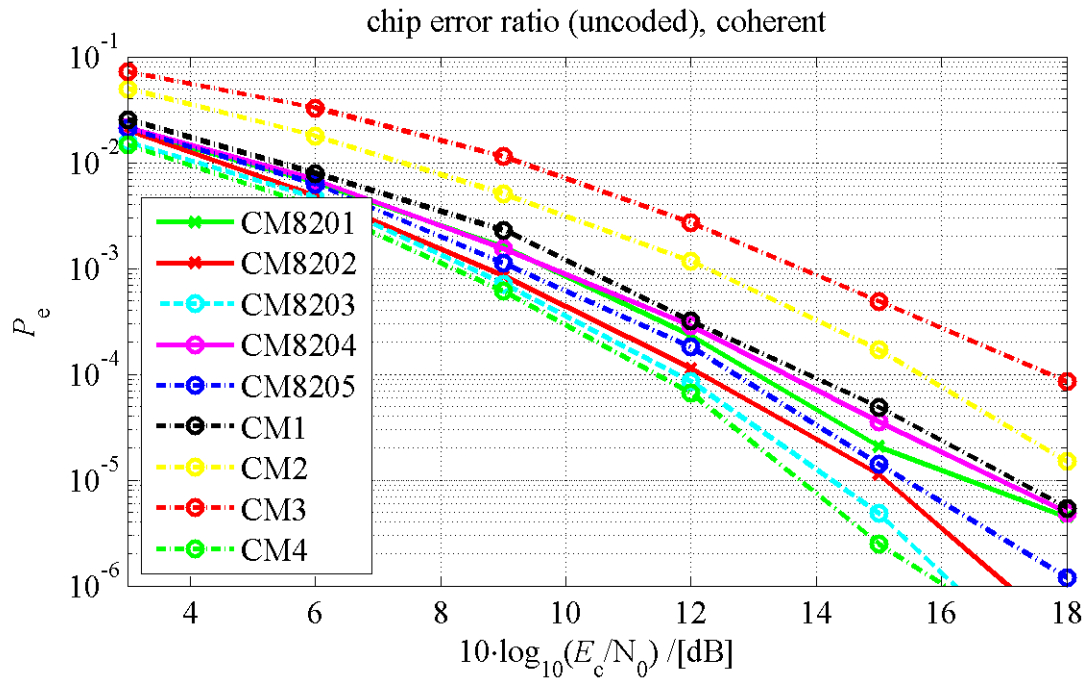


Figure 5-1: Uncoded chip error ratio for coherent BPSK Rx

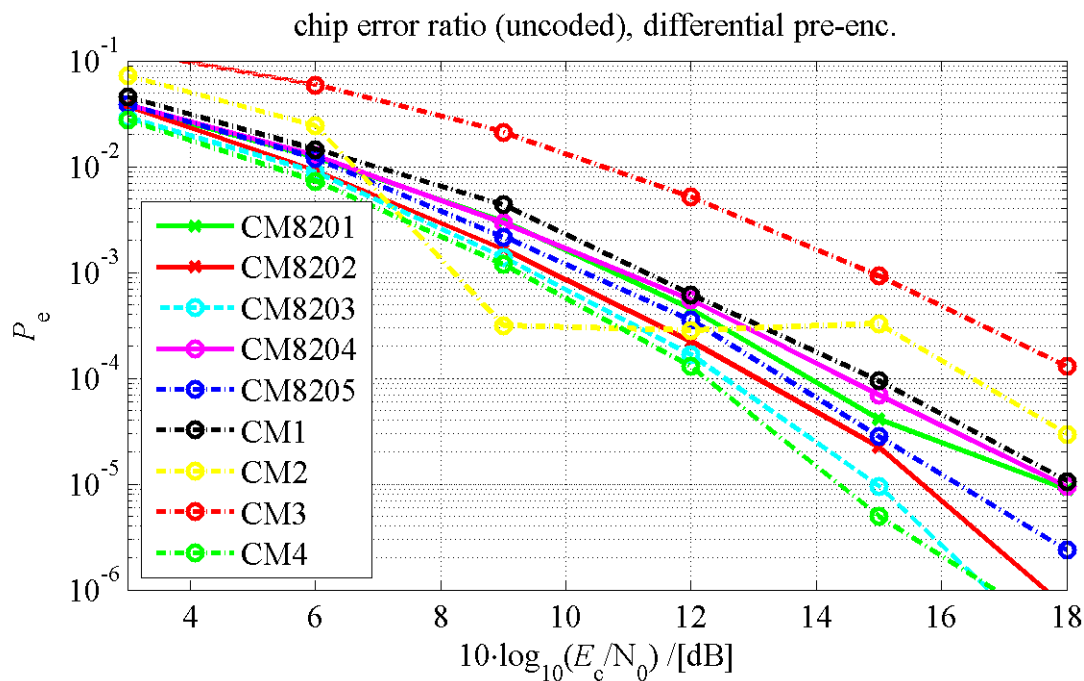


Figure 5-2: Uncoded chip error ratio for non-coherent Rx with differentially pre-encoded DBPSK

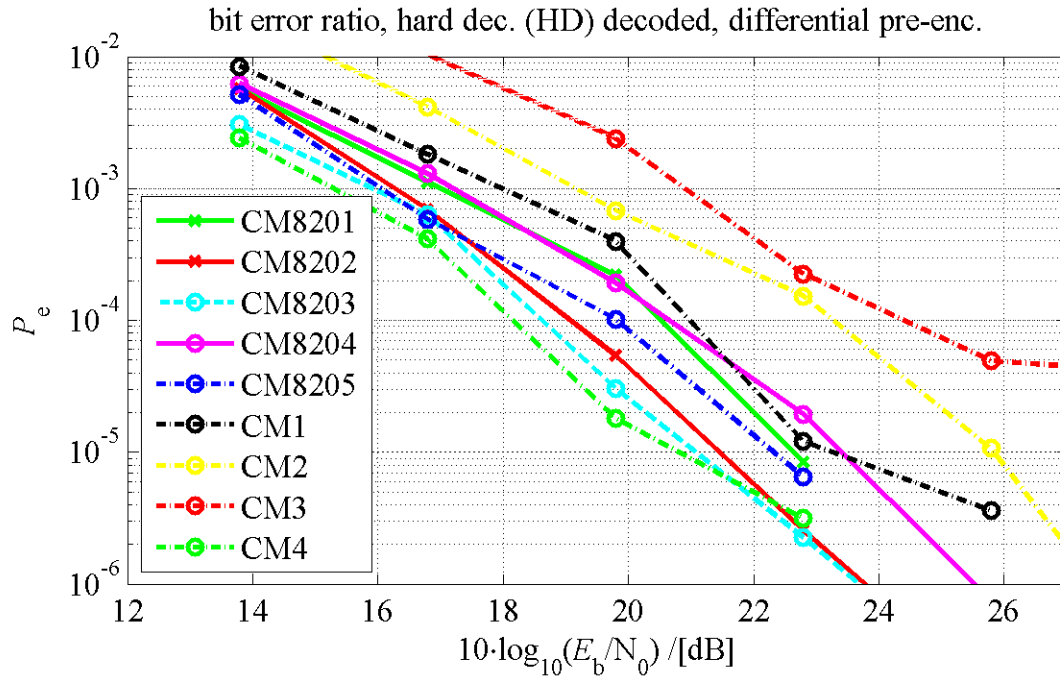


Figure 5-3: Coded bit error ratio for non-coherent Rx with hard decision (HD) decoder, spreading factor $N_{PN} = 12$, differentially pre-encoded DBPSK

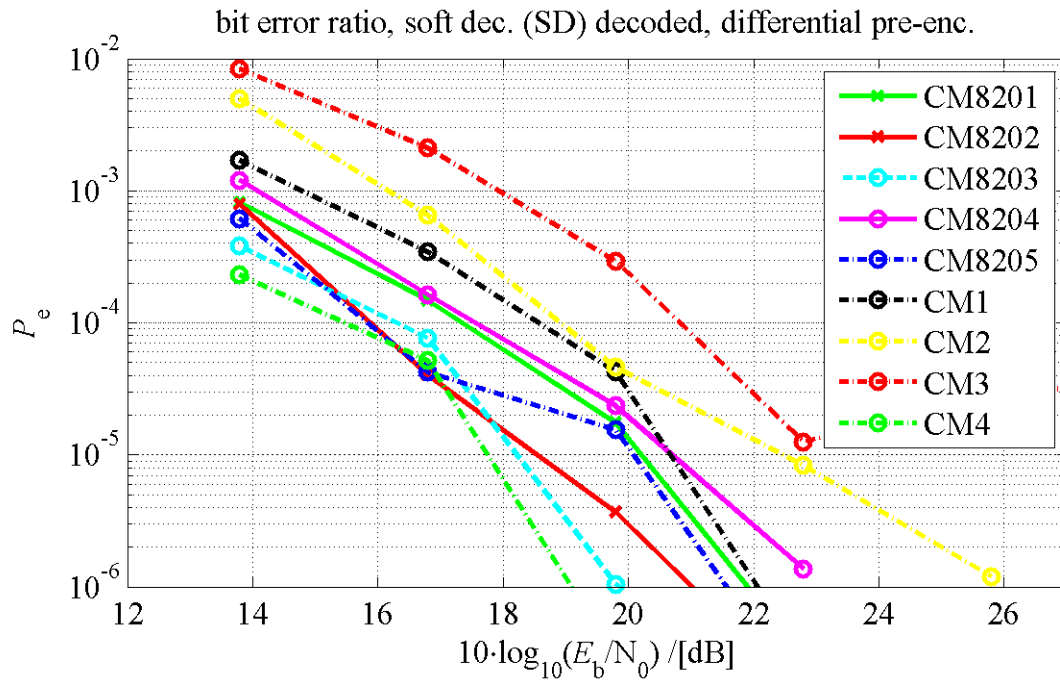


Figure 5-4: Coded bit error ratio for non-coherent Rx with soft decision (SD) decoder, spreading factor $N_{PN} = 12$, differentially pre-encoded DBPSK

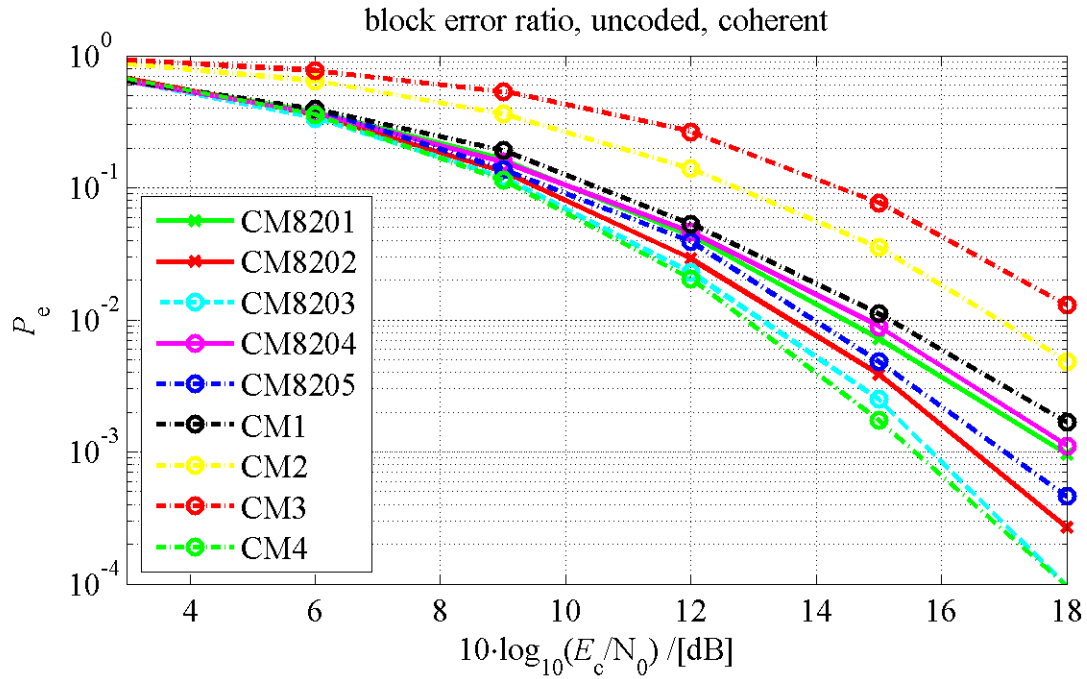


Figure 5-5: Uncoded block error ratio for coherent BPSK Rx, block length $N_c = 3072$

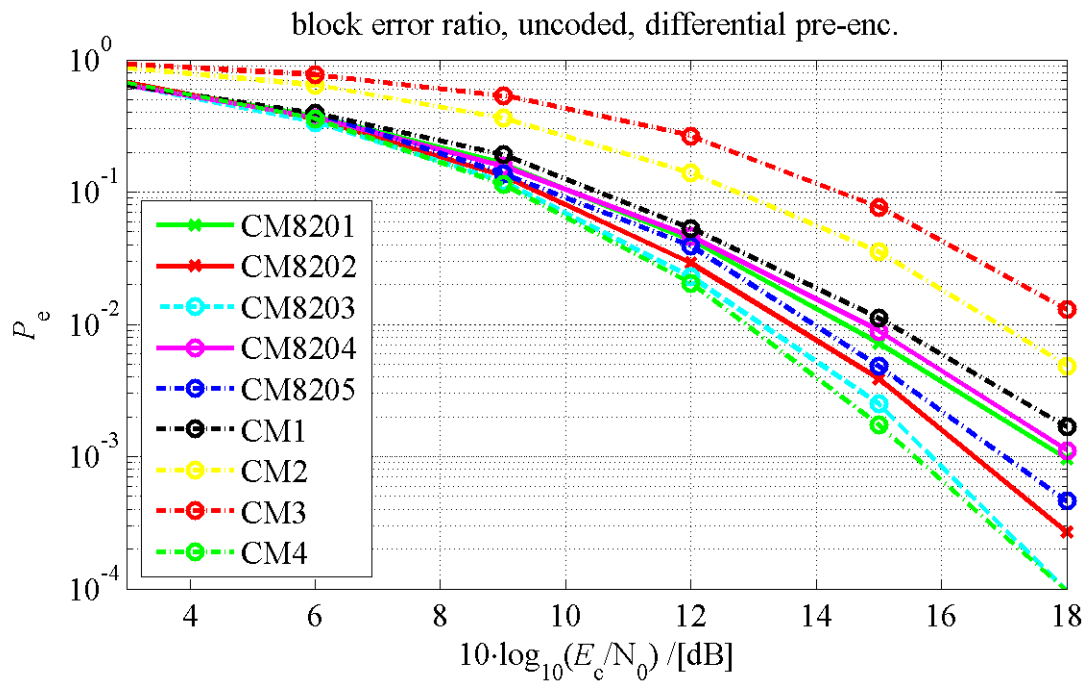


Figure 5-6: Uncoded block error ratio for non-coherent Rx, differentially pre-encoded DBPSK, block length $N_c = 3072$

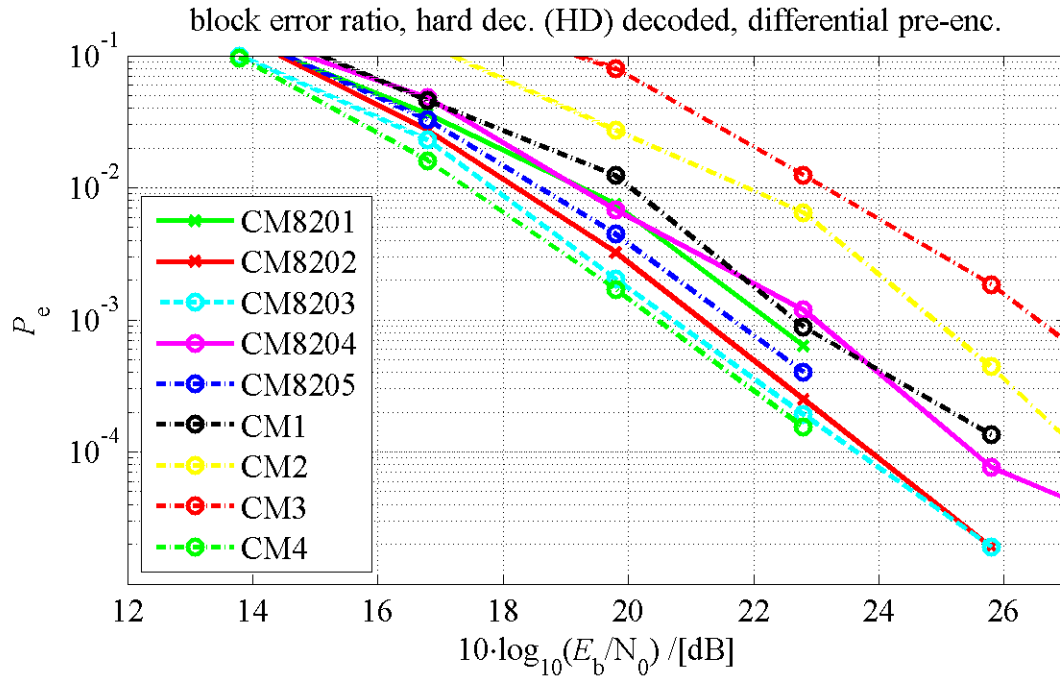


Figure 5-7: Coded block error ratio for non-coherent DBPSK Rx with hard decision (HD) decoder, spreading factor $N_{PN} = 12$, block length $N_c = 3072$

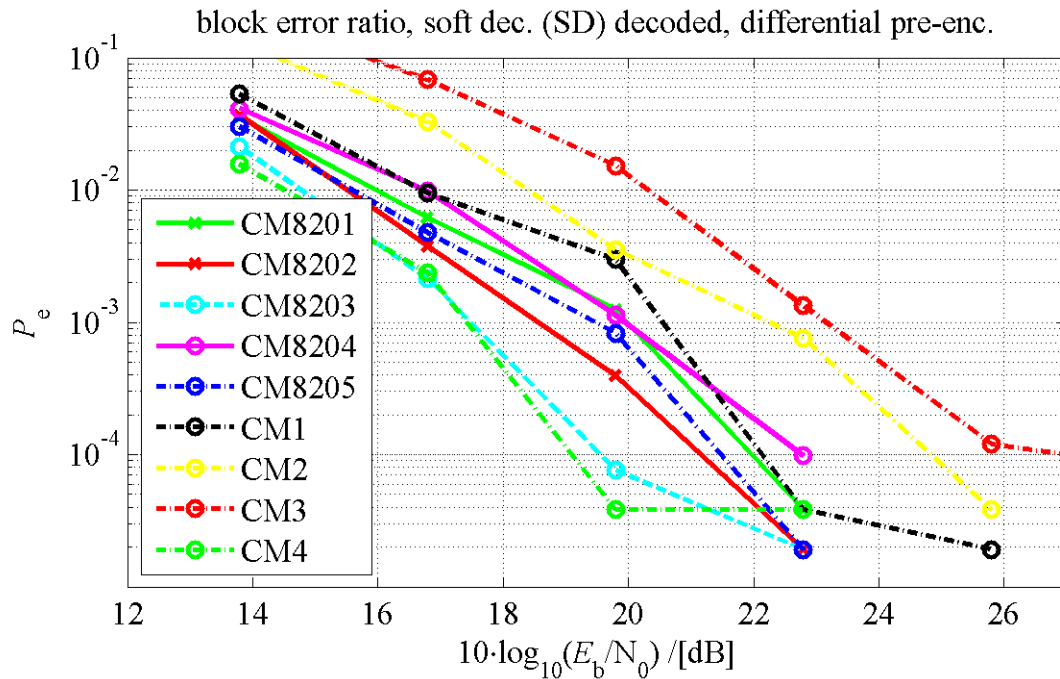


Figure 5-8: Coded block error ratio for non-coherent DBPSK Rx with soft decision (SD) decoder, spreading factor $N_{PN} = 12$, block length $N_c = 3072$

5.3 Discussion

The non-coherent receiver with pre-encoded DBPSK has usually double as many chip errors or uncoded bit errors than the coherent BPSK receiver, because every chip error leads to one additional inherited error in the next chip. This yields also a significant performance degradation, if channel

coding or spreading is used in a non-coherent receiver structure. Only in case of the uncoded block error ratios in Figure 5-5 and Figure 5-6 the performances of the coherent BPSK receiver and the non-coherent receiver with pre-encoded DBPSK are the same. This is caused by the fact that a block is counted as error-prone, independently on the number of bit errors in this block. The number of bit error in the block may be one or two, the inherited error in the next chip does not worsen the block error.

6 Conclusion

In this document, a simulation environment has been presented. The software simulator is based on the system specifications of the Impulse-Radio-UWB LDR platform, and on the EUWB channel models from the automotive sector WP8b. The system simulation environment is now available, including the reliable channel models as they are based on measurements of real world scenarios. Performance simulation results have been carried out for different environments by using EUWB and IEEE channel models. The performance results depend on the utilized channel model. Comparing the EUWB channel models with the reference channels from IEEE 802.15, it can be seen that in all scenarios of the EUWB channels, the system performance is always better than in the worst case reference channel from IEEE 802.15 and worse than in the best case reference channel from IEEE 802.15.

References

- [1] S. Zeisberg, V. Schreiber: "EUWB - Coexisting Short Range Radio by Advanced Ultra-Wideband Radio Technology," *ICT Mobile and Wireless Communications Summit*, Stockholm, June 2008.
- [2] URL of EUWB consortium: <http://www.euwb.eu>
- [3] J. Hasch, "Scenario description for automotive environment applications," *Deliverable D8b.1 of the Integrated Project – EUWB*, June 2008.
- [4] J. Foerster, Ed., "Channel Modeling Sub-committee Report Final," IEEE802.15-02/490; <http://ieee802.org/15/>.
- [5] A. Saleh, and R. Valenzuela, "A Statistical Model for Indoor Multipath Propagation", *IEEE journal on selected areas in communications*, vol. SAC-2, no. 2, Feb. 1987, pp. 128–137.
- [6] S. Gaier et al., "Channel model for complex automotive scenarios (in-car)," *Deliverable D8b.4 of the Integrated Project – EUWB*, October 2009.
- [7] R. Zetik et al., "Application-specific MIMO-UWB channel measurements and parameter extraction (final)," *Deliverable D3.1.2b of the Integrated Project – EUWB*, July 2009.
- [8] S. Gaier et al., "Verification of channel model by measurement," *Deliverable D8b.5 of the Integrated Project – EUWB*, May 2010.
- [9] M. Pendergrass, "Empirically Based Statistical Ultra-Wideband Channel Model," IEEE P802.15-02/240-SG3a.
- [10] J. Foerster and Q. Li, "UWB Channel Modeling Contribution from Intel," IEEE P802.15-02/279-SG3a.
- [11] M. Pezzin et al., "LDR-LT platform requirements, feasibility analysis and specification", *ICT EUWB Deliverable D7.1.1b*, October 2009.
- [12] B. Denis et al., "A LDR IR-UWB Receiver Architecture Based on 1-Bit Direct Sampling," *IST Mobile and wireless communications summit*, Mykonos, June 2006.

Acknowledgement

The EUWB consortium would like to acknowledge the support of the European Commission partly funding the EUWB project under Grant Agreement FP7-ICT-215669 [1],[2].